Journal of Alloys and Compounds 685 (2016) 551–558

HPSTAR 300_2016

Contents lists available at ScienceDirect

Journal of Alloys and Compounds

journal homepage: http://www.elsevier.com/locate/jalcom

Pressure-induced electron phase transitions of α-As_2Te_3

Yuhang Zhang [a], Yanmei Ma [a, **], Aihui Geng [b], Chunye Zhu [a], Guangtao Liu [a], Qiang Tao [a], Fangfei Li [a], Qinglin Wang [c], Yan Li [a], Xin Wang [a], Pinwen Zhu [a, *]

[a] State Key Laboratory of Superhard Materials, College of Physics, Jilin University, Changchun 130012, China
[b] Changchun Institute of Optics, Fine Mechanics and Physics, Chinese Academy of Sciences, Changchun 130022, China
[c] Center for High Pressure Science and Technology Advanced Research, Changchun 130012, China

ARTICLE INFO

Article history:
Received 3 March 2016
Received in revised form
15 May 2016
Accepted 28 May 2016
Available online 30 May 2016

Keywords:
As_2Te_3
High-pressure
Phase transition
Electronic band structure
Thermoelectric property
Bulk modulus

ABSTRACT

Using a diamond-anvil cell (DAC), we conducted *in situ* angle dispersive X-ray diffraction (ADXRD) up to 47.6 GPa at room temperature to evaluate the structural stability of α-As_2Te_3. A reversible structural transition was observed at between 17.4 and 36.3 GPa. The high-pressure structure is solved by a γ-Bi_2Te_3-type monoclinic phase ($C2/c$, γ-As_2Te_3). Reliable structural analyses, such as Rietveld refinement of the powder x-ray data, were provided, which show that the previously reported high-pressure β-As_2Te_3 phase is not existed. It is worth mentioning that twice pressure-induced electron phase transitions were revealed in α-As_2Te_3 at about 3 and 6 GPa, which cause the striking fluctuation in thermoelectric property at that pressures.

© 2016 Elsevier B.V. All rights reserved.

1. Introduction

The A_2B_3 (A = Bi, Sb, As; B=O, S, Se, Te) series compounds have stimulated enormous research activity, because of their exceptional thermoelectric properties [1]. More recently, the α-Bi_2Se_3, α-Bi_2Te_3 and α-Sb_2Te_3 compounds have been theoretically proposed and experimentally exhibited as topological insulators (TIs), are insulators in their bulk, but show a metallic state at their surfaces [2–5]. Pressure has been served as a powerful tool in tuning the crystalline structures and the physical properties of these compounds [6–23]. As an example, Bi_2Te_3 and Sb_2Te_3 undergo a common pressure-induced structural phase transition sequence: R-$3m$ → $C2/m$ → $C2/c$ → disordered Im-$3m$, respectively [6,20]. In particular, pressure-induced electronic topological transitions can result in significant enhancements of thermoelectric properties in these materials [1,24–26]. Note that topological superconductors were also realized by application of external pressure in this series [12,23,27–30].

In recent decades, As_2Te_3, as an important member of the A_2B_3 series, has been extensively investigated on its electrical threshold, memory devices, thermoelectric properties, conduction mechanism, and pressure-induced amorphous to crystalline transition [31–38]. Monoclinic α-As_2Te_3 (space group $C2/m$) is the stable form of arsenic telluride (As_2Te_3) at ambient pressure [39–41]. To the best of our knowledge very scant attention has been taken to α-As_2Te_3 at high pressure. The unique high-pressure studies of α-As_2Te_3 mentioned a structural transformation to β-As_2Te_3 at about 6 GPa, leading to a dramatic change in its thermoelectric property [31,32]. However, reliable analyses, such as Rietveld refinement of the powder x-ray data, were not provided thorough. On the other hand, the β-As_2Te_3 phase (R-$3m$) is isostructural to α-Bi_2Te_3 and α-Sb_2Te_3 phase [42]; furthermore, the recent calculation research reported that a uniaxial strain induced β-As_2Te_3 transformed from a trivial insulator to a Weyl semimetal, and then to a topological insulator [43]. Therefore, intriguing topological nature may be expected in the transition process in α-As_2Te_3 phase under high pressure.

Here, we report twice pressure-induced electron phase transitions in α-As_2Te_3 by room temperature synchrotron angle-dispersive X-ray diffraction (ADXRD) measurements up to

* Corresponding author.
** Corresponding author.
E-mail addresses: ymma@jlu.edu.cn (Y. Ma), zhupw@jlu.edu.cn (P. Zhu).

http://dx.doi.org/10.1016/j.jallcom.2016.05.309
0925-8388/© 2016 Elsevier B.V. All rights reserved.

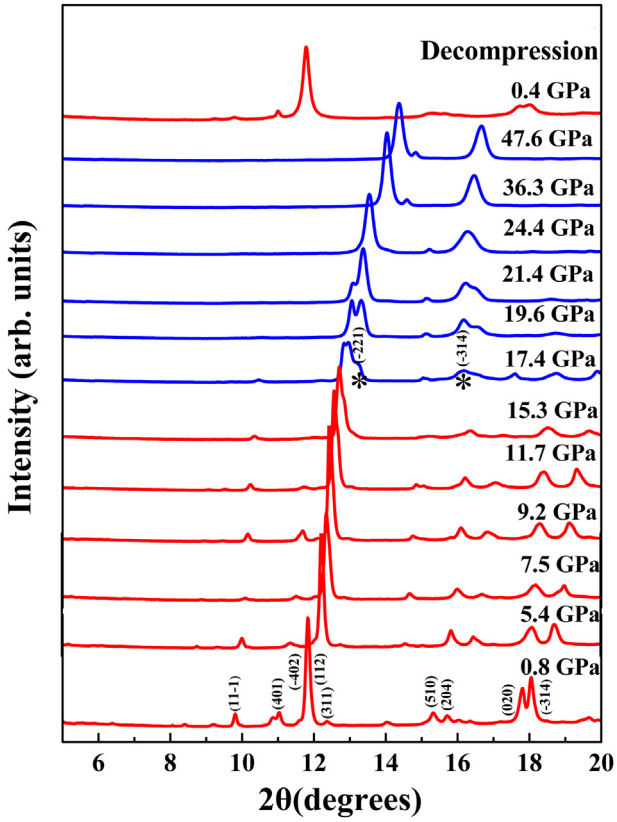

Fig. 1. ADXRD patterns collected at various pressures for As_2Te_3 with an incident wavelength = 0.6199 Å. The peaks marked with asterisks are the diffraction peaks for new phase.

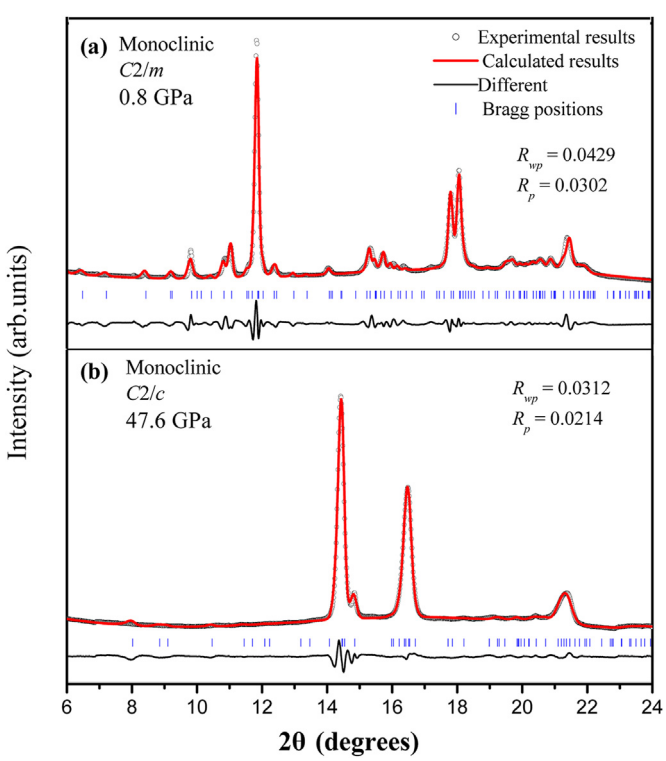

Fig. 2. Rietveld full-profile refinement of the diffraction pattern collected on compression at (a) 0.8 GPa ($C2/m$, α-As_2Te_3 phase), (b) 47.6 GPa ($C2/c$, γ-As_2Te_3 phase) at room temperature.

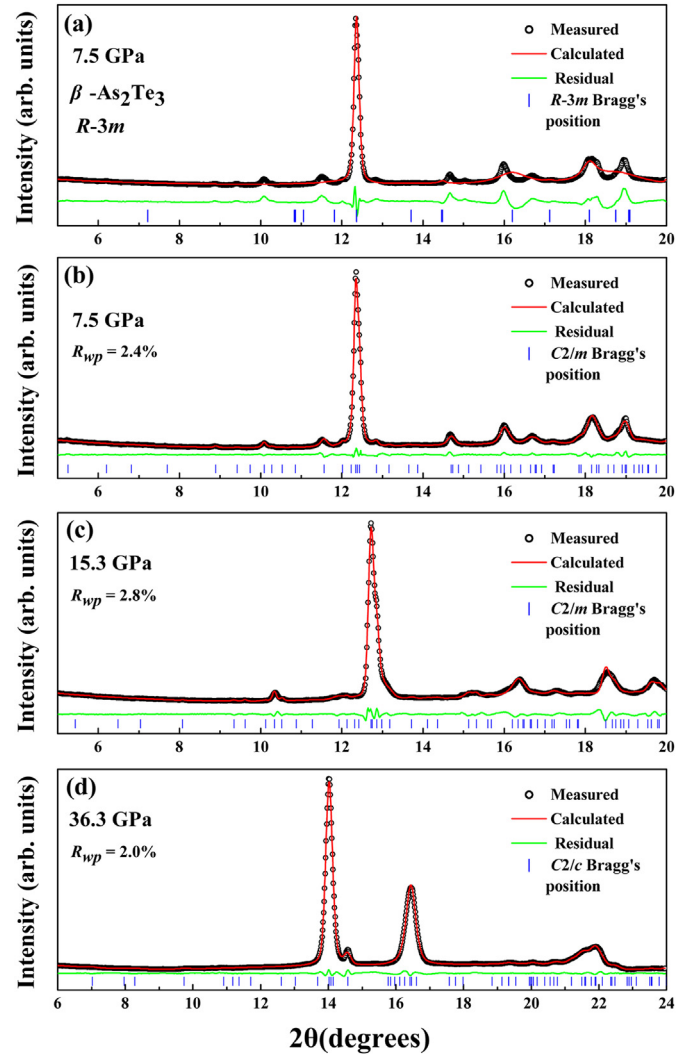

Fig. 3. Rietveld full-profile refinement of the diffraction pattern collected on compression at (a) 7.5 GPa (R-3m, β-As_2Te_3 phase), (b) 7.5 GPa ($C2/m$, α-As_2Te_3 phase), (c) 15.3 GPa ($C2/m$, α-As_2Te_3 phase) and (d) 36.3 GPa ($C2/c$, γ-As_2Te_3 phase) at room temperature.

47.6 GPa, using a diamond-anvil cell (DAC), in conjunction with first-principles calculations.

2. Experimental details

Commercially available As_2Te_3 powder (Alfa-Aesar, 99.999%) was in poly-crystalline form. Pressure was generated by a symmetric DAC with 300 μm diamond culet size. A hole of 120 μm diameter was drilled in the middle of a preindented stainless steel gasket of 50 μm thickness and served as the sample chamber. Pressure was determined by using ruby fluorescence technique [44]. A methanol-ethanol-water (16:3:1) mixture was employed as the pressure transmitting medium. *In situ* high-pressure ADXRD experiments at room temperature were carried out in the 4W2 High-Pressure Station of Beijing Synchrotron Radiation Facility (BSRF) using monochromatic wavelength of 0.6199 Å. The diffraction patterns were collected on an image plate detector (MAR-345). The average acquisition time was 300 s. The integration to conventional 2θ-intensity data was carried out with the FIT2D software [45]. Rietveld refinements were performed using the GSAS-EXPGUI

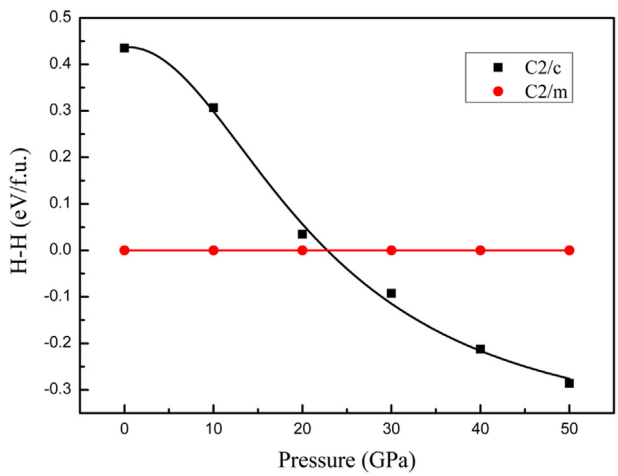

Fig. 4. Enthalpy curves of the γ-phase as function of pressure (relative to the α-phase).

package [46]. We performed structure prediction through a global minimization of free energy surfaces merging ab initio total-energy calculations via CALYPSO methodology. For the first-principles calculations, the density functional theory with the Perdew-Burke-Ernzerhof exchange-correlation as implemented in the Vienna Ab initio Simulation Package (VASP) code [47] and the generalized gradient approximation (GGA) [48] is implemented on a projector augmented wave (PAW) basis [49,50]. The PAW method based upon the frozen core approximation with $4s^24p^3$ and $5s^25p^4$ electrons as valence for As and Te, respectively, was adopted. $10 \times 10 \times 10$ Monkhorst-Pack k point meshes were adopted for α and γ phase, respectively, and Brillouin zone sampling was performed with a 300 eV energy cutoff, ensuring convergence of the total energy within 1 meV/atom.

3. Results and discussion

3.1. Structure properties

The selected ADXRD patterns are shown in Fig. 1. It can be seen that the pressure-induced structural transition started at about 17.4 GPa, where new peaks appeared. Furthermore, the analysis of ADXRD patterns reveal that the phase transition is not completed until 36.3 GPa and it is reversible with relaxing the pressure. Fig. 2a clearly illustrates the initial phase is assigned to the α-As_2Te_3 structure [39]. The experimental crystallographic information, such as lattice parameters and atomic coordinates, are shown in the Supplementary material. To solve the new high-pressure structure, the CALYPSO methodology [51] was used and the best fitting was achieved for a γ-Bi_2Te_3 isostructural monoclinic phase (*C*2/*c*, γ-As_2Te_3). The predicted structural information of γ-As_2Te_3 phase is collected in the Supplementary material. Fig. 2b shows the Rietveld refinement for the γ-As_2Te_3 phase at 47.6 GPa, which has a good fitting with the ADXRD pattern. The relative experimental results of Rietveld refinement were shown in the Supplementary material. Due to there are no new peaks until the pressure up to 17.4 GPa (see Fig. 1). Therefore, the previously reported transition from α-As_2Te_3 phase to β-As_2Te_3 phase at about 6 GPa was not occurred. Moreover, in order to verify the reported phase transition at about 6 GPa, reliable experiments, such as Rietveld refinement of the powder x-ray data, have been carried out. It is known that β-As_2Te_3 phase

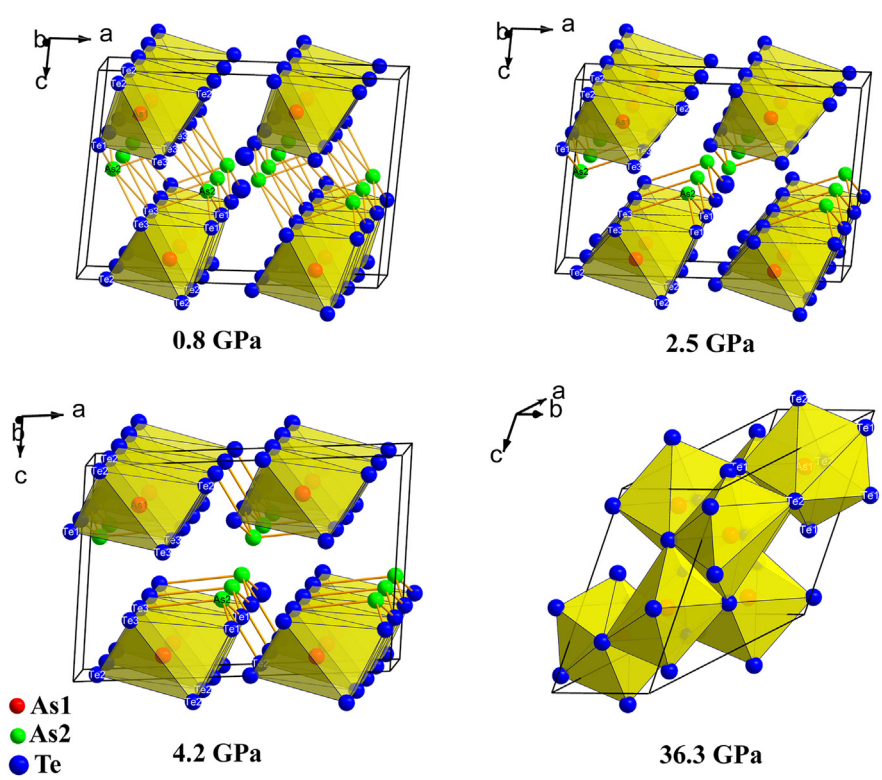

Fig. 5. Schematic crystal structures of the α-As_2Te_3 phase at 0.8 GPa, 2.5 GPa and 4.2 GPa, respectively. Structure of γ-As_2Te_3 phase at 36.3 GPa.

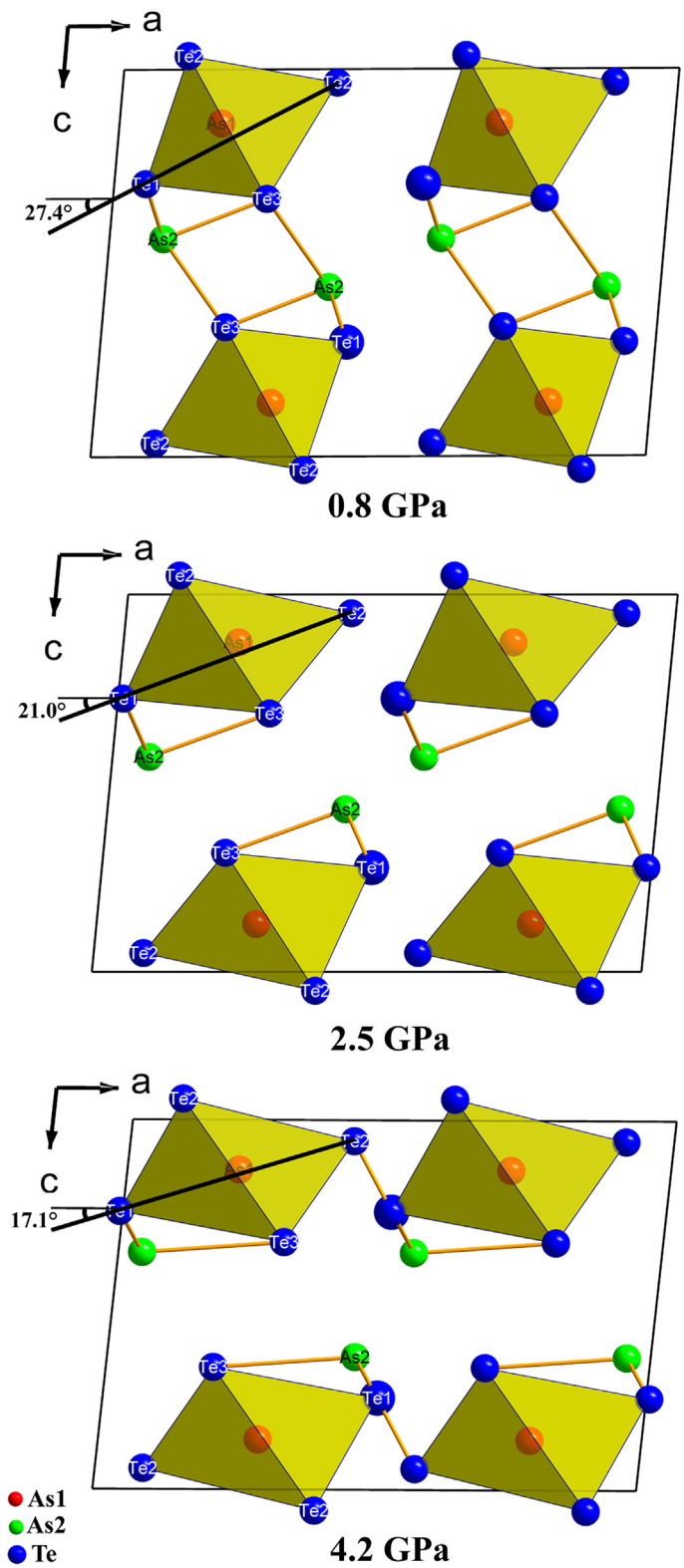

Fig. 6. Schematic representation of the α-As_2Te_3 phase (for viewing along *b* axis) at 0.8, 2.5 and 4.2 GPa, respectively.

crystallizes in the *R*-3*m* symmetry (space group No.166) with the lattice parameters $a = 4.05\ (8)$ (Å), $c = 29.59\ (0)$ (Å), $Z = 3$ [41–43]. Because the Rietveld refinement of ADXRD pattern at 7.5 GPa with the β-As_2Te_3 phase shows a very bad fitting result (see Fig. 3a). In contrast, as seen in Fig. 3b and 3c, the α-As_2Te_3 structure can perfectly fitted the observed ADXRD pattern at 7.5 GPa and even up to 15.3 GPa. Therefore, the results of Rietveld refinements further verified that the α-As_2Te_3 phase is stable up to 15.3 GPa and the

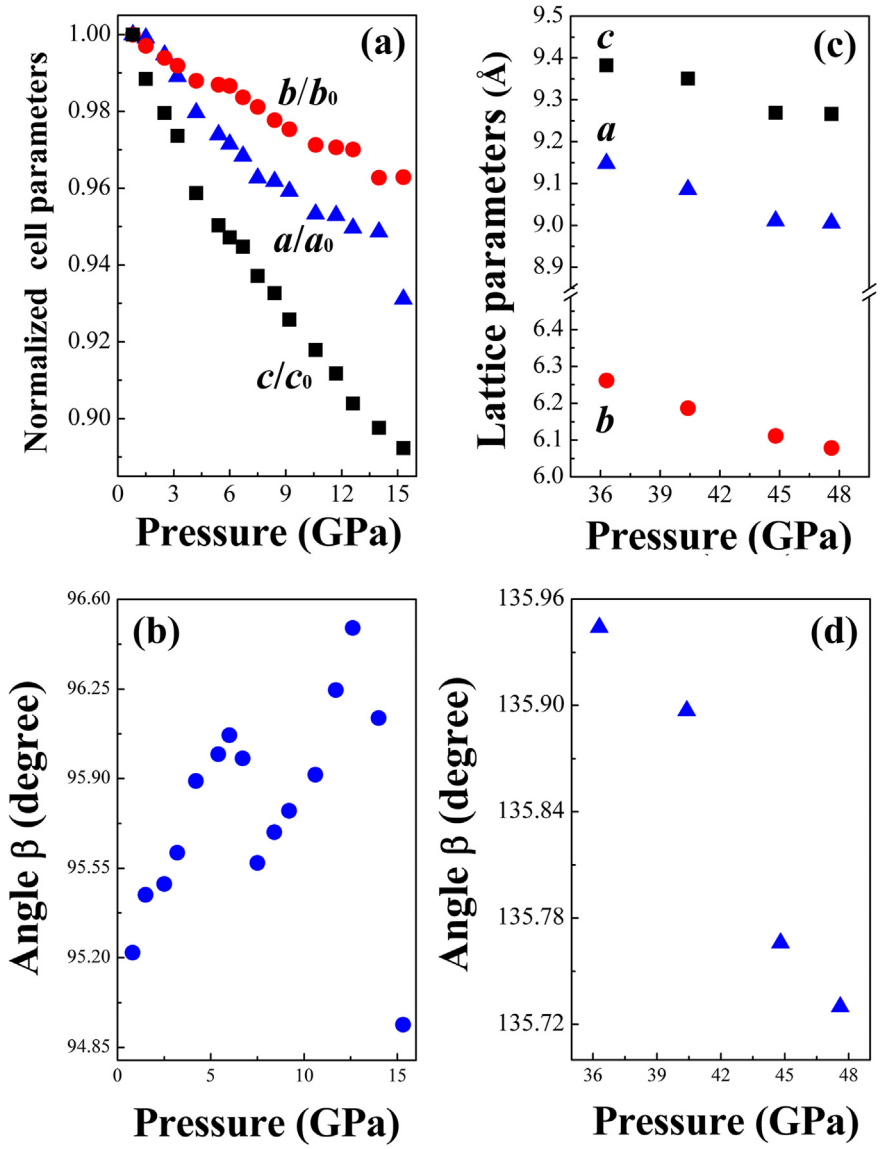

Fig. 7. (a) Normalized cell parameters of the α-As_2Te_3 phase, (b) lattice parameters of the γ-As_2Te_3 phase. Angle β of (c) the α-As_2Te_3 and (d) the γ-As_2Te_3 phase. Errors given by the GSAS EXPGUI package are smaller than the marker sizes.

proposed transition to β-As_2Te_3 phase at 6 GPa is not existed. The Rietveld refinement of pattern at 36.3 GPa with the γ-As_2Te_3 phase achieved a good fitting (Fig. 3d), which further shows that the phase transition is not completed until 36.3 GPa. The relative experimental results of Rietveld refinements are located in the Supplementary material. The static enthalpies ($T = 0$ K) for the γ phase relative to the α phase as a function of pressure are plotted in Fig. 4. The calculated results show that the α phase transformed into the γ phase at about 23.0 GPa (Fig. 4), which is consistent with our initial experimental phase transition pressure 17.4 GPa. Therefore, based on the results of the structure predictions, Rietveld refinements and static enthalpies, the accurate pressure-induced phase transition sequence is determined.

As shown in Figs. 5 and 6, the α-As_2Te_3 structure has two crystallographically inequivalent As sites: for As1, it forms edges-sharing As1Te6 octahedra along *b* axis; As2 links with five Te at below 2.5 GPa. Under further compression, the As1Te6 octahedra rotated around *b* axis, which make the coordination number of As2 with nearby Te decreases to three at 2.5 GPa and then increases to four at above 4.2 GPa, respectively. It is evident from Fig. 5, apart from the observed rotation of the As1Te6 octahedra, the obvious distortions also been seen in the As1Te6 octahedra with increasing pressure. As seen in Fig. 5, the γ phase can be described as stacked blocks of AsTe7 polyhedra linked by edges-sharing.

The evolution of the normalized cell parameters in α-As_2Te_3 phase is presented in Fig. 7a. The contraction of the lattice parameters is rather anisotropic. For instance, according to our experiments, *c* and *a* directions are more compressible than *b* direction. This fact is essentially due to the spatial arrangements of As1Te6 octahedra, which closely squeezes each other along *b* direction and leaves much space along *c* and *a* directions (see Fig. 5). As seen in Fig. 8, the compressibility of lattice parameter ratios undergoes intense fluctuation at around 6 GPa, which may be attributed to a pressure-induced second-order isostructural phase transition. Besides, the angle β also displays notable changes in compressibility near 6 GPa (Fig. 7b). For the overlapping diffraction

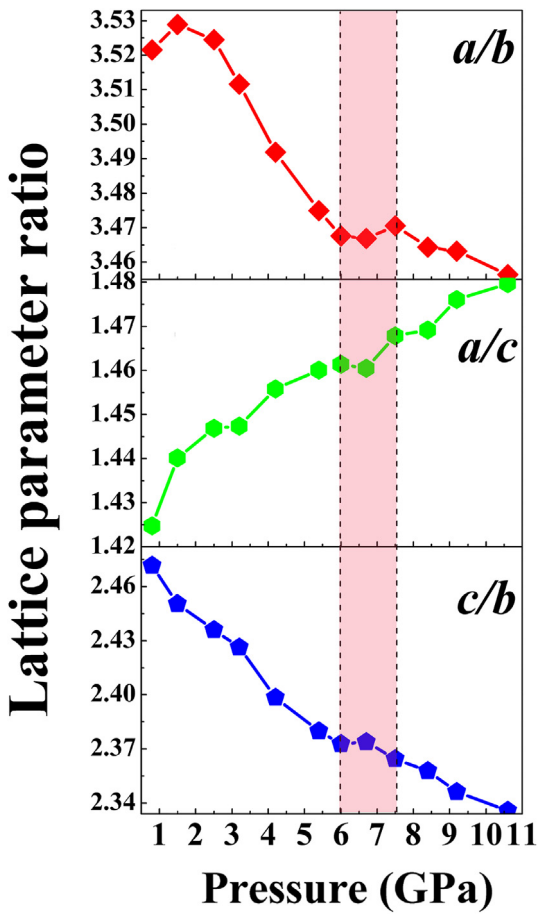

Fig. 8. Lattice parameter ratios of the α-As_2Te_3 phase (from 0.5 to 10.6 GPa). The solid lines are guide for the eyes. Errors given by the GSAS EXPGUI package are smaller than the marker sizes.

peaks in the pressure region of mixed phases, it is difficult to identify the peak positions of the γ phase exactly. Therefore, we only display the lattice parameters of the γ phase angel β at above

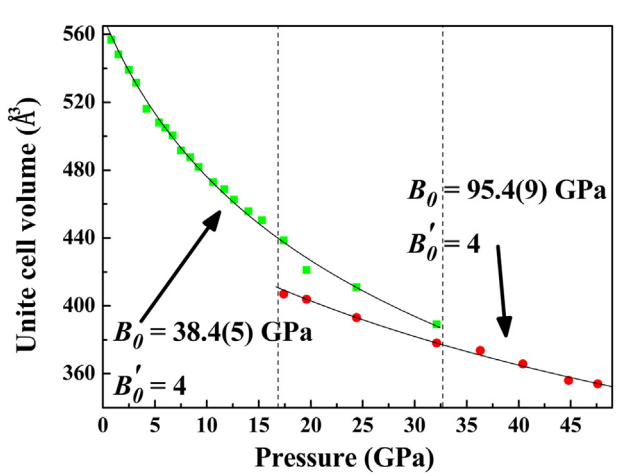

Fig. 9. The experimental pressure dependence of per four formula units volume for the α-phase and the γ-phase. Errors given by the GSAS EXPGUI package are smaller than the marker sizes.

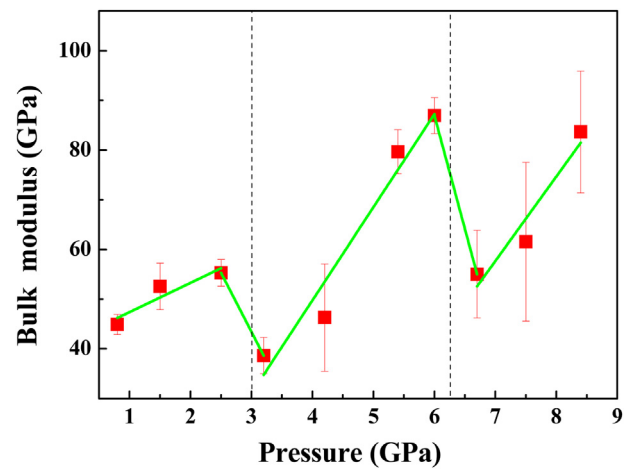

Fig. 10. Bulk modulus K *vs.* pressure in the α-As_2Te_3 phase (from 0.5 to 8.4 GPa).

36.3 GPa (see Fig. 7c and 7d).

The volume per four formula units as a function of pressure is shown in Fig. 9. A Birch-Murnaghan equation of state (EOS) was used to fit our pressure-volume data [52]. By fixing first-pressure derivative B_0'=4, we obtained B_0 = 38.4 (5) GPa and V_0 = 570.5 (7) Å^3 for the α phase, which is in good agreement with the calculated B_0 of 42.7 GPa in the recent report [41]. The lower B_0 are most likely due to the higher compressibility of c and a directions in the α-phase. The compressibility behaviour of γ phase is described by the following characteristic parameters: B_0 = 95.4 (9) GPa, V_0 = 469.9 (7) Å^3 and B_0' fixed to 4 (see Fig. 9).

A more accurate analysis of the experimental results can be done thanks to the local bulk modulus, $K = -V(dP/dV)$, as a function of pressure in Fig. 10. The pressure coefficient of bulk modulus was different at about 3 and 6 GPa, respectively. This observation further verifies that α-As_2Te_3 experiences twice pressure-induced second-order isostructural phase transitions at about 3 and 6 GPa, respectively.

3.2. Electronic properties

In order to investigate the effects of pressure-induced second-order isostructural phase transitions on the electronic band structures, we carried out first-principles calculations, which is useful to shed light on the notable change in thermoelectric property of α-As_2Te_3 at 3 and 6 GPa. Deng et al. reported α-As_2Te_3 is an indirect band-gap semiconductor (Eg = 0.32 eV) at ambient pressure, with the valence-band maximum (VBM) located between Z and V point and the conduction-band minimum (CBM) located at M point [41]. However, as shown in Fig. 11a, the isostructural phase I is a direct band-gap semiconductor (Eg = 0.20 eV) at 5.4 GPa with VBM and CBM at V point. Based on the indirect-to-direct transition on the electronic band structures, the first isostructural phase transition is identified as an electronic phase transition in α-As_2Te_3. Due to the reduction in band-gap under pressure, an increase of carrier concentration can be obtained. Moreover, due to the indirect-to-direct band-gap crossover, the phonon-assisted intervalley scattering was suppressed [53]. Therefore, the observed enhancement in thermoelectric power of α-As_2Te_3 at about 3 GPa was attributed to this electronic phase transition [32].

Besides, as shown in Fig. 11b, the isostructural phase II is an indirect band-gap semiconductor (Eg = 0.42 eV) at 7.5 GPa with VBM located between A and Γ point and CBM at M point. Due to the

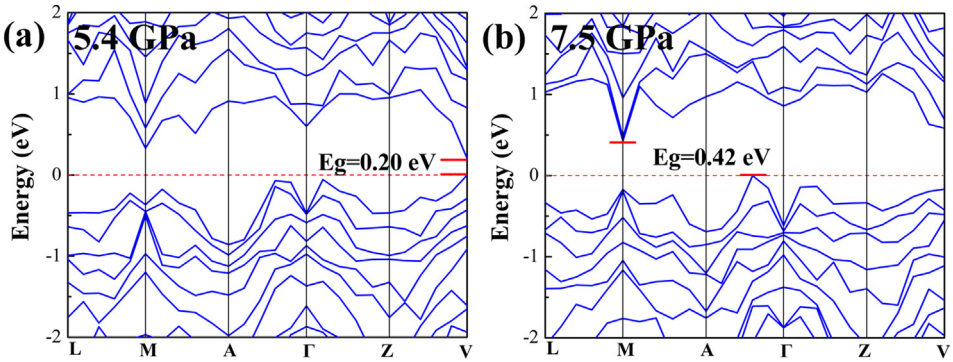

Fig. 11. Calculated energy band structures of (a) isostructural phase I and (b) isostructural phase II.

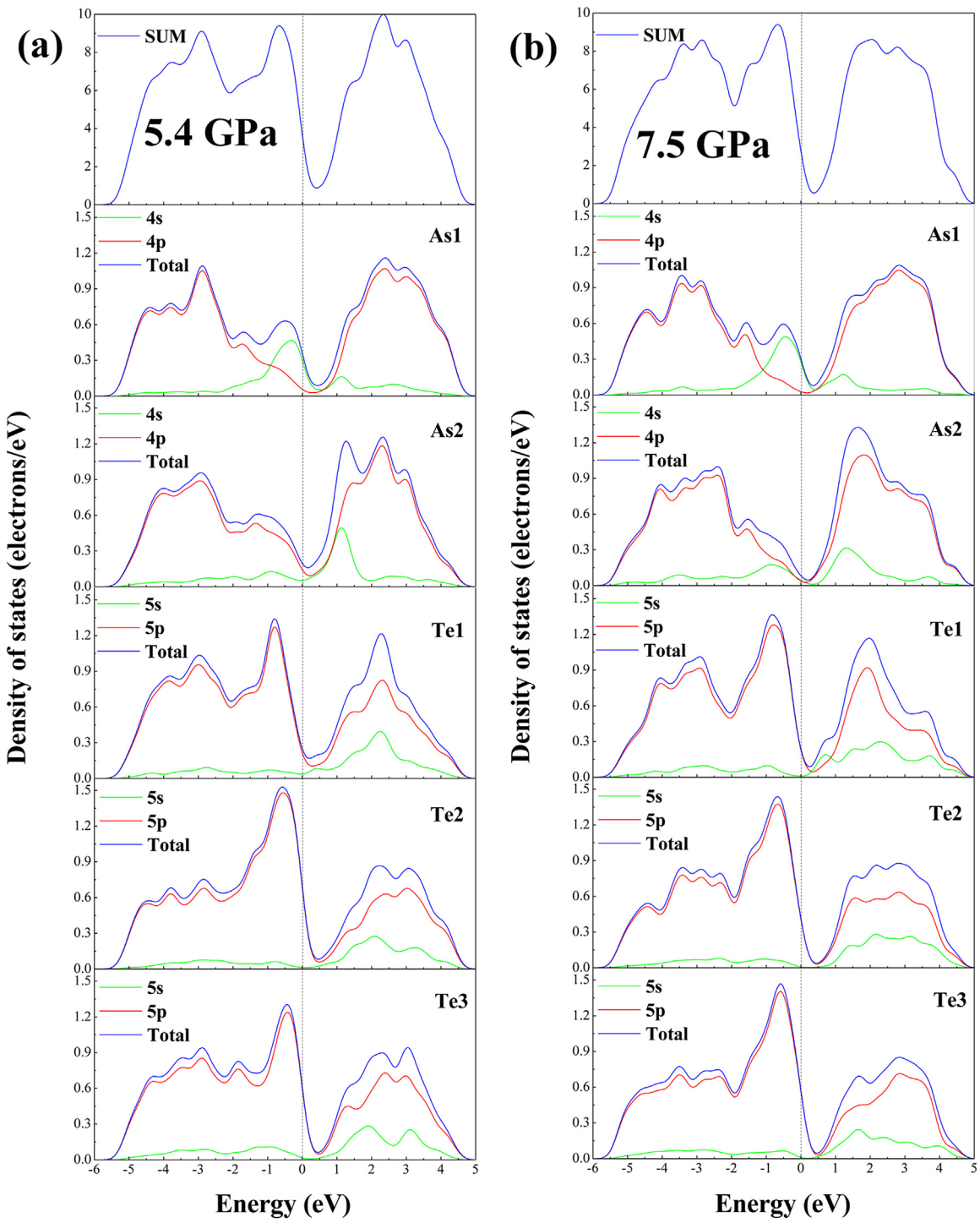

Fig. 12. The sum and partial density of states of (a) isostructural phase I and (b) isostructural phase II.

direct-to-indirect transition, the second isostructural phase transition is also an electronic phase transition. As shown in Fig. 12, after the second electronic phase transition, there is a remarkable decrease in the sum electron density of state (DOS) near the Fermi energy level, which was mainly caused by the reduced contribution from As2, Te1 and Te2 atoms. Three factors can account for the striking decay of thermoelectric property after the second electronic phase transition: (a) The thermoelectric property is very sensitive to the degeneracy of the energy bands near the Fermi level. The reduced sum DOS near the E_F leads to a decrease in thermoelectric power. (b) The increased band-gap results in the decrease in carrier concentration. (c) Due to the direct-to-indirect transition, the phonon-assisted intervalley scattering of transport electron at the CBM was extremely significant.

4. Conclusions

In summary, we investigated the high-pressure structural transition of α-As_2Te_3 up to 47.6 GPa at room temperature. The accurate structural transition sequence is determined: α-phase ($C2/m$) started to transform into the γ-As_2Te_3 phase ($C2/c$) at 17.4 GPa. Reliable structural analyses, such as Rietveld refinement of the powder x-ray data, were provided. The reported structural transition from α to β phase in As_2Te_3 at about 6 GPa has not been found. On the other hand, pressure-induced electron phase transitions in α-As_2Te_3 were uncovered at about 3 and 6 GPa, which can perfectly explain the observed change of thermoelectric property.

Acknowledgments

This work was supported by the National Natural Science Foundation of China (Grant 11304114 and 51172091), Program for New Century Excellent Talents in University (NCET-12-0240), and Jilin Province Science and Technology Development Program, China (20130101023JC). Part of this experimental work was performed at 4W2 beamline, Beijing Synchrotron Radiation Facility (BSRF).

Appendix A. Supplementary data

Supplementary data related to this article can be found at http://dx.doi.org/10.1016/j.jallcom.2016.05.309.

References

[1] S.V. Ovsyannikov, V.V. Shchennikov, Chem. Mater. 22 (2010) 635.
[2] Y. Chen, J. Analytis, J.-H. Chu, Z. Liu, S.-K. Mo, X.-L. Qi, H. Zhang, D. Lu, X. Dai, Z. Fang, Science 325 (2009) 178.
[3] H. Zhang, C.X. Liu, X.L. Qi, X. Dai, Z. Fang, S.C. Zhang, Nat. Phys. 5 (2009) 438.
[4] X.L. Qi, S.C. Zhang, Rev. Mod. Phys. 83 (2011) 1057.
[5] B. Yan, S.C. Zhang, Rep. Prog. Phys. 75 (2012) 96501.
[6] L. Zhu, H. Wang, Y.C. Wang, J. Lv, Y. Ma, Q.L. Cui, Y. Ma, G.T. Zou, Phys. Rev. Lett. 106 (2011) 145501.
[7] M. Einaga, A. Ohmura, A. Nakayama, F. Ishikawa, Y. Yamada, S. Nakanoet, Phys. Rev. B 83 (2011) 92102.
[8] M. Einaga, Y. Tanabe, A. Nakayama, A. Ohmura, F. Ishikawa, Y. Yamada, J. Phys. Conf. Ser. 215 (2010) 12036.
[9] M.K. Jacobsen, S.V. Sinogeikin, R.S. Kumar, A.L. Cornelius, J. Phys, Chem. Sol. 73 (2012) 1154.
[10] G.K. Pradhan, A. Bera, P. Kumar, D.V.S. Muthu, A.K. Sood, Solid State Commun. 152 (2012) 284.
[11] R. Vilaplana, O. Gomis, F.J. Manjon, A. Segura, E. Perez-Gonzalez, P. Rodriguez-Hernandez, A. Munoz, J. Gonzalez, V. Marin-Borras, V. Munoz-Sanjos, Phys. Rev. B 84 (2011) 104112.
[12] J.L. Zhang, S.J. Zhang, H.M. Weng, W. Zhang, L.X. Yang, Q.Q. Liu, S.M. Feng, X.C. Wang, R.C. Yu, L.Z. Cao, Proc. Natl. Acad. Sci. U. S. A. 108 (2011) 24.
[13] S.J. Zhang, J.L. Zhang, X.H. Yu, J. Zhu, P.P. Kong, S.M. Feng, Q.Q. Liu, L.X. Yang, X.C. Wang, L.Z. Cao, W.G. Yang, L. Wang, H.K. Mao, Y.S. Zhao, H.Z. Liu, X. Dai, Z. Fang, S.C. Zhang, C.Q. Jin, J. Appl. Phys. 111 (2012) 112630.
[14] G.T. Liu, L. Zhu, Y.M. Ma, C.L. Lin, J. Liu, J. Phys, Chem. C 117 (2013) 10045.
[15] J. Zhao, H. Liu, L. Ehm, D. Dong, Z. Chen, G. Gu, J. Phys. Condens. Matter 25 (2013) 125602.
[16] J.J. Hamlin, J.R. Jeffries, N.P. Butch, P. Syers, D.A. Zocco, S.T. Weir, Y.K. Vohra, J. Paglione, M.B. Maple, J. Phys. Condens. Matter 24 (2012) 35602.
[17] A. Segura, V. Panchal, J.F. Sánchez-Royo, V. Marín-Borrás, V. Muñoz-Sanjosé, P. Rodríguez-Hernández, A. Muñoz, E. Pérez-González, F.J. Manjón, J. González, Phys. Rev. B 85 (2012) 195139.
[18] R. Vilaplana, D. Santamaria-Perez, O. Gomis, F.J. Manjón, J. González, A. Segura, A. Muñoz, P. Rodríguez-Hernández, E. Pérez-González, V. Marín-Borrás, V. Muñoz-Sanjosé, C. Drasar, V. Kucek, Phys. Rev. B 84 (2011) 184110.
[19] J. Zhao, H. Liu, L. Ehm, Z. Chen, S. Sinogeikin, Y. Zhao, G. Gu, Inorg. Chem. 50 (2011) 11291.
[20] Y. Ma, G. Liu, P. Zhu, H. Wang, X. Wang, Q. Cui, J. Liu, Y.M. Ma, J. Phys. Condens. Matter 24 (2012) 475403.
[21] S.M. Souza, C.M. Poffo, D.M. Triches, J.C. de Lima, T.A. Grandi, A. Polian, M. Gauthier, Phys. B 407 (2012) 3781.
[22] O. Gomis, R. Vilaplana, F.J. Manjón, P. Rodríguez-Hernández, E. Pérez-González, A. Muñoz, V. Kucek, C. Drasar, Phys. Rev. B 84 (2011) 174305.
[23] J. Zhu, J.L. Zhang, P.P. Kong, S.J. Zhang, X.H. Yu, J.L. Zhu, Q.Q. Liu, X. Li, R.C. Yu, R. Ahuja, W.G. Yang, G.Y. Shen, H.K. Mao, H.M. Weng, X. Dai, Z. Fang, Y.S. Zhao, C.Q. Jin, Sci. Rep. 3 (2013) 2016.
[24] F.J. Manjón, R. Vilaplana, O. Gomis, E. Pérez-González, D. Santamaría-Pérez, V. Marín-Borrás, A. Segura, J. González, P. Rodríguez-Hernández, A. Muñoz, C. Drasar, V. Kucek, V. Muñoz-Sanjosé, Phys. Status Solidi B 250 (2013) 669.
[25] E. Itskevich, L. Kashirskaya, V. Kraidenov, Semiconductors 31 (1997) 276.
[26] C.N. Shekar, D. Polvani, J. Meng, J. Badding, Phys. B 358 (2005) 14.
[27] M.X. Wang, C. Liu, J.P. Xu, F. Yang, L. Miao, M.Y. Yao, C.L. Gao, C. Shen, X. Ma, X. Chen, Z.A. Xu, Y. Liu, S.C. Zhang, D. Qian, J.F. Jia, Q.K. Xue, Science 336 (2012) 52.
[28] P.P. Kong, J.L. Zhang, S.J. Zhang, J. Zhu, Q.Q. Liu, R.C. Yu, Z. Fang, C.Q. Jin, W.G. Yang, X.H. Yu, J.L. Zhu, Y.S. Zhao, J. Phys, Condens. Matter 25 (2013) 362204.
[29] K. Kirshenbaum, P.S. Syers, A.P. Hope, N.P. Butch, J.R. Jeffries, S.T. Weir, J.J. Hamlin, M.B. Maple, Y.K. Vohra, J. Paglione, Phys. Rev. Lett. 111 (2013) 087001.
[30] P.P. Kong, F. Sun, L.Y. Xing, J. Zhu, S.J. Zhang, W.M. Li, Q.Q. Liu, X.C. Wang, S.M. Feng, X.H. Yu, J.L. Zhu, R.C. Yu, W.G. Yang, G.Y. Shen, Y.S. Zhao, R. Ahuja, H.K. Mao, C.Q. Jin, Sci. Rep. 4 (2014) 4.
[31] N. Sakai, H. Fritzsche, Phys. Rev. B 15 (1977) 973.
[32] T.J. Scheidemantel, J.F. Meng, J.V. Badding, J. Phys. Chem. Solids 66 (2005) 1744.
[33] D.M. Chiu, J. Phys. D. Appl. Phys. 16 (1983) 1507.
[34] G. Parthasarathy, E.S.R. Gopal, Bull. Mater. Sci. 7 (1985) 271.
[35] J.B. Vaney, J. Carreaud, G. Delaizir, A. Pradel, A. Piarristeguy, C. Morin, E. Alleno, J. Monnier, A.P. Gonçalves, C. Candolfi, A. Dauscher, B. Lenoir, Adv. Electron. Mater 1 (2015) 1400008.
[36] D.D. Thornburg, J. Electron. Mater 2 (1973) 495.
[37] K. Ramesh, J. Phys, Chem. B 118 (2014) 8848.
[38] C. Morin, S. Corallini, J. Carreaud, J.B. Vaney, G. Delaizir, J.C. Crivello, E.B. Lopes, A. Piarristeguy, J. Monnier, C. Candolfi, V. Nassif, G.J. Cuello, A. Pradel, A.P. Goncalves, B. Lenoir, E. Alleno, Inorg. Chem. 54 (2015) 9936.
[39] G.J. Carron, Acta Crystallogr. 16 (1963) 338.
[40] T.C. Habman, B. Paris, S.E. Miller, H.L. Goefung, J. Phys. Chem. Solids 2 (1957) 181.
[41] H. Deng, J. Alloys Compd. 656 (2016) 695.
[42] S. Toscani, J. Dugue, R. Ollitrault, R. Ceolin, Theor. Chim. Acta 186 (1991) 247.
[43] K. Pal, U.V. Waghmare, App. Phys. Lett. 105 (2014) 062105.
[44] H.K. Mao, J. Xu, P.M. Bell, J. Geophys. Res. 91 (1986) 4673.
[45] A.P. Hammersley, S.O. Svensson, M. Hanfland, A.N. Fitch, D. Hausermann, High. Press. Res. 14 (1996) 235.
[46] A.C. Larson, R.B. Von Dreele, General Structure Analysis System, LANSCE, MS-H805, Los Alamos, New Mexico, 1994.
[47] G. Kresse, J. Furthmüller, Phys. Rev. B 54 (1996) 11169.
[48] J.P. Perdew, K. Burke, M. Ernzerhof, Phys. Rev. Lett. 77 (1996) 3865.
[49] G. Kresse, D. Joubert, Phys. Rev. B 59 (1999) 1758.
[50] P.E. Blöchl, Phys. Rev. B 50 (1994) 17953.
[51] Y. Wang, J. Lv, L. Zhu, Y. Ma, Phys. Rev. B 82 (2010) 094116.
[52] F. Birch, J. Appl. Phys. 9 (1938) 279.
[53] F.J. Manjón, D. Errandonea, A. Segura, V. Muñoz, G. Tobías, P. Ordejón, E. Canadell, Phys. Rev. B 63 (2001) 125330.